Massively parallel pooled screening reveals genomic determinants of nanoparticle-cell interactions

Natalie Boehnke[1,2]†, Joelle P. Straehla[1,2,3,4]†, Hannah C. Safford[1], Mustafa Kocak[2], Matthew G. Rees[2], Melissa Ronan[2], Charles H. Adelmann[5,6,8], Raghu R. Chivukula[6,9], Jaime H. Cheah[1], Hojun Li[1,3,4], David M. Sabatini[1,2,6,7,8], Jennifer A. Roth[2], Angela N. Koehler[1,2,10], Paula T. Hammond[1,11]*

Affiliations:

[1] Koch Institute for Integrative Cancer Research, Massachusetts Institute of Technology; Cambridge, MA, USA.

[2] Broad Institute of MIT and Harvard; Cambridge, MA, USA.

[3] Department of Pediatric Oncology, Dana-Farber Cancer Institute; Boston, MA, USA.

[4] Division of Pediatric Hematology/Oncology, Boston Children's Hospital; Boston, MA, USA.

[5] Cutaneous Biology Research Center, Massachusetts General Hospital Department of Dermatology, Harvard Medical School; Boston, MA, USA.

[6] Whitehead Institute for Biomedical Research; Cambridge, MA, USA

[7] Howard Hughes Medical Institute; Cambridge, MA, USA.

[8] Department of Biology, Massachusetts Institute of Technology; Cambridge, MA, USA.

[9] Division of Pulmonary and Critical Care Medicine, Department of Medicine, Massachusetts General Hospital; Boston, MA, USA.

[10] Department of Biological Engineering, Massachusetts Institute of Technology; Cambridge, MA, USA.

[11] Department of Chemical Engineering, Massachusetts Institute of Technology; Cambridge, MA, USA.

*Corresponding author. Email: hammond@mit.edu

†These authors contributed equally to this work

Abstract:

To accelerate the translation of cancer nanomedicine, we hypothesize that integrated genomic screens will improve understanding of the cellular processes governing nanoparticle trafficking. We developed a massively parallel high-throughput screening method leveraging barcoded, pooled cancer cell lines annotated with multi-omic data to investigate cell association patterns across a nanoparticle library spanning a range of formulations with clinical potential. This approach identified both the materials properties and cell-intrinsic features mediating nanoparticle-cell association. Coupling the data with machine learning algorithms, we constructed genomic nanoparticle trafficking networks and identified nanoparticle-specific biomarkers. We engineered cell lines to validate SLC46A3 as a biomarker whose expression inversely predicts liposomal nanoparticle uptake. Our work establishes the power of massively parallel pooled cell screens and enables the identification and utilization of nanoparticle predictive biomarkers to rationally design nanoformulations for specific patient populations.

Main Text:

Nanoparticle (NP)-based therapeutics have enormous potential for personalized cancer therapy as they can encapsulate a range of therapeutic cargos including small molecules, biologics and, more recently, nucleic acids.[1, 2] Therapy-loaded NPs can be designed to prevent undesired degradation of the cargo, increase circulation time, and direct drugs specifically to target tumors. There have been notable successes in clinical translation of nanomedicines, including liposomal formulations of doxorubicin (Doxil) and irinotecan (Onivyde®).[3] These formulations extend the half-life of the active agent and have the potential to lower toxicity, but do not efficiently accumulate in tumors.[4, 5]

Efforts to improve NP accumulation in tumors via active targeting motifs have been met with limited success, both in the laboratory and the clinic.[1, 6] While progress has been made in understanding how specific physical and chemical NP properties affect trafficking and uptake, comprehensive evaluation of multiple NP parameters in combination has thus far been elusive. Additionally, tissue and cellular heterogeneity make it prohibitively challenging to gain a holistic understanding of which NP properties dictate successful trafficking and drug delivery.[7, 8] Once these NP parameters are considered in combination, the number of unique formulations to test increases exponentially, particularly as comparisons across several systems need to be drawn. A further barrier is the need to adapt the nanoparticle formulation of each encapsulated therapy for a given drug or target, as each formulation has its own unique biological fate.[8] As therapies continue to increase in molecular complexity, new nanocarrier formulations capable of delivering these entities will need to be developed and examined for their unique trafficking properties.

We and others have designed panels of NPs to elucidate the structure-function relationships to cellular targeting and uptake.[9-14] However, there is a need to equally consider the influence of biological heterogeneity on these interactions. In the era of precision medicine, with the desire to deliver molecularly targeted and gene-based therapies to specific subcellular compartments within cancer cells, it is imperative to holistically probe the structure-function relationship of NPs as they relate to cellular interactions.

Inspired by recent advancements in cancer genomics,[15] we postulated that applying these same techniques to the study of cancer nanomedicine would uncover both the cell- and NP-specific features mediating efficient targeting and delivery. The combination of pooled screening with multi-omic annotation has accelerated target discovery and uncovered previously unrecognized mechanisms of action in small molecule screens. Specifically, in the Profiling Relative Inhibition in Mixtures (PRISM) method, DNA-barcoded mixtures of cells have recently been used for multiplexed viability screening. In cell line pools grouped by doubling time, 500 barcoded cell lines have been screened against tens of thousands of compounds to identify genotype-specific cancer vulnerabilities.[16, 17]

To comprehensively capture pan-cancer complexities and enable the statistical power to link NP association with cell intrinsic characteristics, we developed a competitive phenotypic screen to assess NP-cell associations of a curated NP library across hundreds of cancer cell lines simultaneously. By pooling and plating 488 DNA barcoded cancer cell lines in a single well, we screened the interactions of a range of NP formulations with varied core compositions, surface chemistries, and diameters. We identified that NP core composition has a dominating influence on cell-specific interactions of the studied parameters. Coupling our biomarker findings with k-means clustering, we constructed genomic interaction networks associated with NP engagement, enabling the identification and connection of genes associated with the binding, recognition, and subcellular trafficking of distinct NP formulations. Moreover, through the use of univariate analyses and random forest algorithms, we identified that the gene *SLC46A3* holds significant value as a predictive, NP-specific biomarker, with expression inversely correlated to liposomal NP uptake. Our work adds a new dimension to the study of cancer nanomedicine, demonstrating the power of pooled screening with a diverse NP library to advance the field.

nanoPRISM: screening nanoparticle association with pooled cell lines

To screen hundreds of cancer cell lines simultaneously for NP-cancer cell line association patterns, we cultured pooled PRISM cells and incubated them with fluorescent NPs. We then implemented a fluorescence-activated cell sorting (FACS) adaptive gating strategy to sort cell populations into four bins (quartiles, A-D) based on fluorescence signal as a proxy for the extent of NP-cell association (Figure 1A). Experimental parameters were optimized to ensure sufficient cell number and barcode representation post-cell sorting (Figure S1) and NPs were incubated for 4 and 24 hours.

For this screen, we designed a modular NP library to capture the effects of NP core composition, surface chemistry, and size on cell interactions. This panel of 35 NPs encompassed both clinical and experimental formulations. Specifically, anionic liposomes were formulated and electrostatically coated with cationic poly-L-arginine (PLR) followed by a series of polyanions.[18-22] The polyanions were selected for their synthetic (polyacrylic acid, PAA), semisynthetic (poly-L-aspartate, PLD; poly-L-glutamate, PLE), or natural (hyaluronate, HA; dextran sulfate, DXS; fucoidan, FUC; alginate, ALG; chondroitin sulfate, CS) origin as well as the inclusion of both carboxylate and sulfate ions.[23-25] These same electrostatic coatings were used to modify polymeric NP cores (polylactide-*co*-glycolide, PLGA) to test the effects of core composition on NP-cell interactions. We optimized formulations to obtain a diameter of approximately 100 nm for the liposome and PLGA formulations as the similar sizes would enable cross-core comparisons. We also included commercially manufactured fluorescent carboxylate- and sulfate-modified polystyrene (PS) nanoparticles in a range of diameters from

20-200 nm, enabling study of particle size and surface chemistry. Because of the clinical importance of polyethylene glycol (PEG)-containing formulations,[26] PEGylated versions of liposome, PLGA, and PS particles were prepared, including the drug-free versions of two commercial formulations, liposomal doxorubicin (Doxil) and liposomal irinotecan (Onyvide®). All of the nanoparticles examined exhibited negative or neutral net charge, as the focus of this work is on systemic nanoparticle delivery systems. Positively charged nanoparticles have been shown to undergo nonspecific charge interactions with cells and proteins, leading to toxicity and premature clearance *in vivo*.[27] Dynamic light scattering (DLS) was used to characterize the diameter, zeta potential, and polydispersity index (Figure 1B, Tables S1-S2) of this NP library.

To ensure that our methods led to robust and meaningful data we selected an anti-epidermal growth factor receptor (EGFR) antibody as an active targeting control. A nonlethal EGFR antibody or IgG isotype control was covalently incorporated onto a liposome via a PEG tether.[28]

After incubation with the NP library and fluorescence-activated cell sorting, cells were lysed, and the DNA barcodes were amplified, sequenced, and deconvoluted according to previously detailed protocols.[16, 29] After quality control analysis of technical (n=2) and biologic (n=3) replicates, all 488 cell lines met quality control measures and were carried forward for downstream analyses (Figure S2, Supplementary Text).

A probabilistic model was developed and applied to the data to infer the relative distribution of each cell line into the pre-determined bins (A-D) for each NP formulation. The probability of a cell from a given cell line falling into a given bin is used to represent those distributions, i.e., $P_A + P_B + P_C + P_D = 1$ (Figure 1C-D). The technical details and the model's implementation are presented in the Supplementary Text section. Given the concordance of the inferred probabilities among the biologic replicates (Figure S3), we collapsed the replicates through their arithmetic average. Probabilities were then summarized using a weighting factor alpha (α) to calculate a weighted average (WA) for each NP-cell line pair: $WA = -\alpha P_A - P_B + P_C + \alpha P_D$ in which a higher WA implies higher NP-cell association and vice versa (Figure 1E). We trialed a range of weighting factors ($\alpha = 2$, 10, 20 and 100) and found that downstream results were unchanged with the higher α values (Figure S4), and therefore, $\alpha = 2$ was used for subsequent analyses.

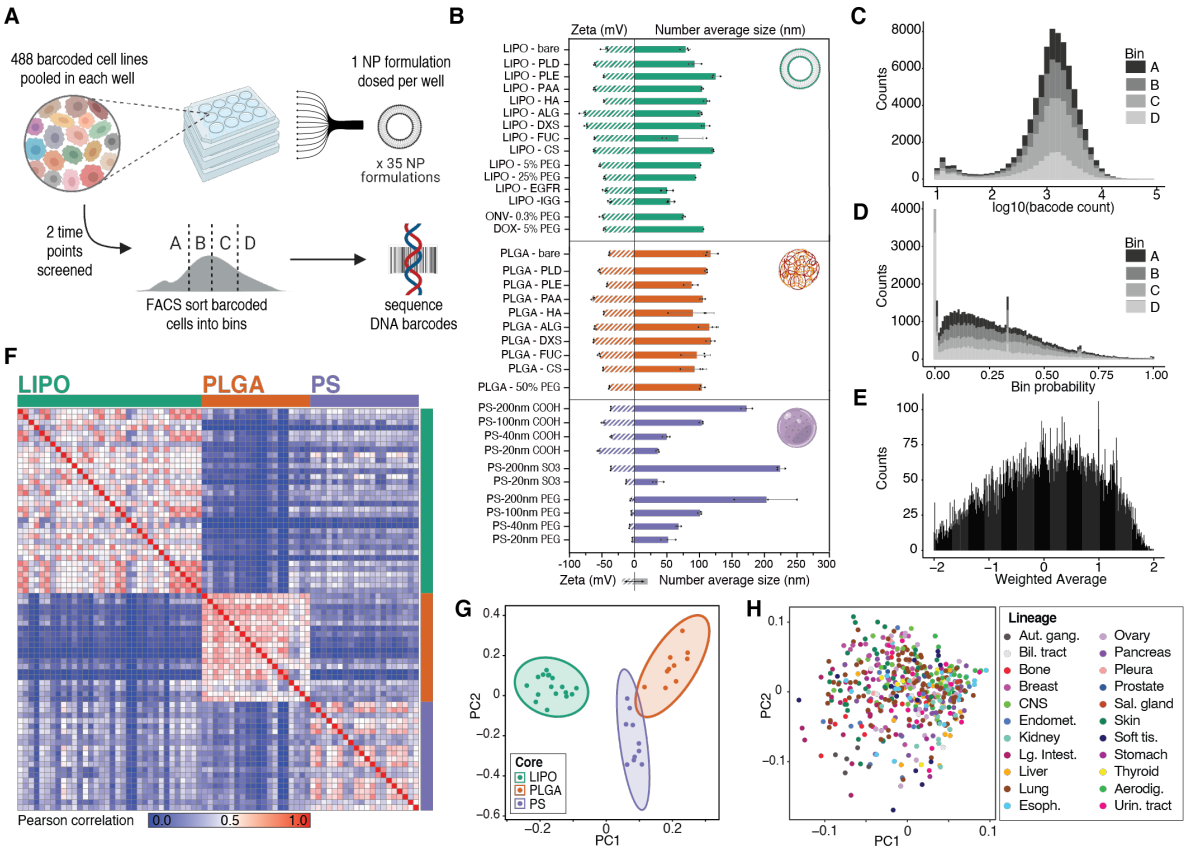

Figure 1. Assessing NP-cell interactions across hundreds of cancer cell lines simultaneously. (**A**) Schematic of the nanoPRISM assay: NPs are incubated with pooled cancer cells before fluorescence-activated cell sorting (FACS) by NP-association and sequencing of DNA barcodes for downstream analyses. (**B**) Characterization of the diameter and zeta potential of the NP library via dynamic light scattering. Data is represented as the mean and standard deviation of three technical repeats. (**C**) Raw data from the screen was obtained in the form of barcode counts, with similar numerical distribution of barcodes in each bin, represented as a stacked histogram. (**D**) Accounting for baseline differences in barcode representation yields the probability (P) that each cell line will be found in a particular bin. (**E**) Probabilities are collapsed into a single weighted average (WA) for each NP-cell line pair. (**F**) A similarity matrix collapsing WA values for 488 cell lines reveals clusters of NP formulations with the same core formulation. (**G-H**) Principal component analysis (PCA) of NP-cell line WA values at 24 h confirms distinct clustering of NP formulations based on core composition but cell lines do not form clusters, indicating lineage does not significantly influence NP-cancer cell interactions.

Cancer cells distinguish nanoparticles based on core composition

Pearson-based unsupervised hierarchical clustering of pairwise WAs identified NP core material as a strong determinant of cell association, with the three core materials tested (liposomal, PLGA and PS) forming distinct clusters (Figure 1F and S5A). This result was unexpected as we hypothesized surface chemistry to be a larger predictor of NP-cell interactions. Principal component analysis (PCA) similarly identified these core specific trends at both the 4 and 24 hour time points (Figures 1G and S5B). Further analysis within each core

material did reveal surface chemistry dependent trends, though they were more subtle than core-based clustering (Figure S6).

In contrast, no clusters were apparent when PCA was performed based on cell line, indicating that cancer cells of the same lineage did not have similar NP-association trends (Figure 1H, Figure S5C). Heterogeneity in NP-cell association in proliferating cells has been attributed to various aspects of cell growth and metabolism.[30-33] To ensure that differential cell proliferation did not confound our results, we performed a parallel growth experiment with the same pooled cells and found no correlation between estimated doubling time and WA (Figure S7).

Cell-intrinsic features mediate nanoparticle trafficking

We applied data from the Cancer Cell Line Encyclopedia (CCLE)[34, 35] to identify genomic features that act as predictive biomarkers for NP-cell association. To do this, we employed both univariate analyses and a random forest algorithm to correlate the baseline molecular features of each cell line (cell lineage; gene copy number; messenger RNA, microRNA, protein or metabolite abundance; function-damaging, hotspot or missense mutations) with NP association.

EGFR-targeting compounds identify relevant biomarkers with high confidence

Using univariate analysis for all CCLE features, we identified EGFR gene expression and protein abundance as the two most significantly correlated hits ($q = 4x\ 10^{-100}$ and $q= 4x10^{-76}$, respectively) with anti-EGFR antibody, but much less significantly ($q = 6\ x\ 10^{-9}$ and $q = 4\ x\ 10^{-10}$, respectively) associated with the isotype control (Figure 2A, top panels).

In EGFR-conjugated liposomes, these same hits were also identified more significantly ($q=6x10^{-21}$ and $q=2x10^{-18}$, respectively) than the IgG control ($q = 3\ x\ 10^{-9}$ and $q = 3\ x\ 10^{-6}$, respectively) (Figure 2A, bottom panels). The statistical significance of EGFR biomarkers was lower for the antibody-conjugated liposome than the free antibody, which may be due to steric blockage introduced by covalently linking an antibody to a NP surface that may interfere with binding to its target.[36] Thus, we demonstrated the ability to quantitatively compare expected biomarker targets of both free antibodies and antibody-conjugated NPs using our platform. This method of analysis will provide therapeutic insights in the design of antibody-drug conjugates, specifically in evaluating the effects of conjugation site or linker chemistry.

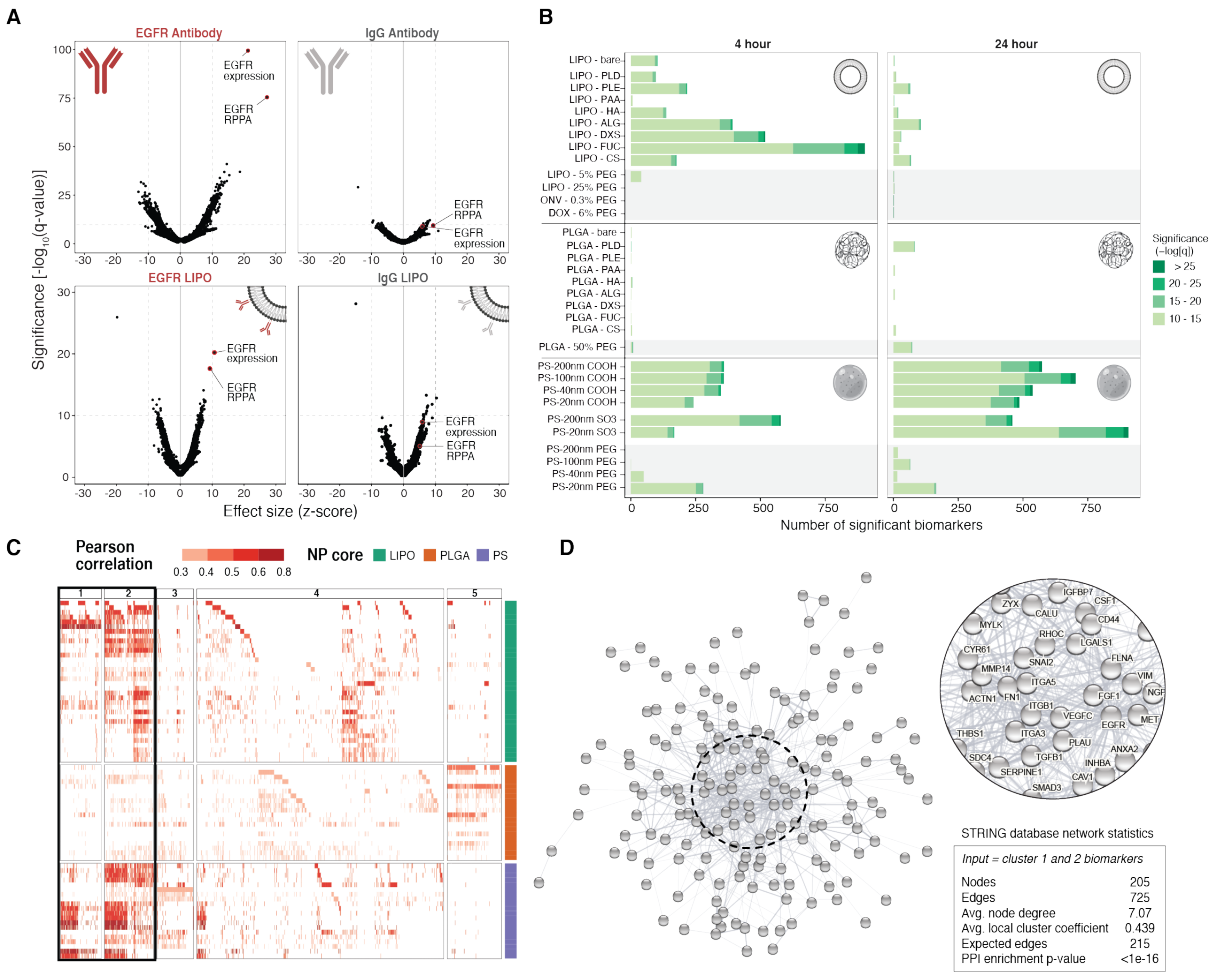

Figure 2. Correlative genomic analysis identifies expected validation biomarkers as well as hundreds of formulation- and time-dependent biomarkers. (**A**) Univariate analysis reveals EGFR gene expression and protein abundance (via reverse phase protein array; RPPA) to be strongly and positively correlated with high anti-EGFR association (top left). EGFR-related markers are much less significant in the isotype control (top right). The same EGFR-related hits, in addition to NP specific markers, are observed for antibody-conjugated liposomes (bottom row). (**B**) Univariate analysis identifies genomic features correlated with NP association. All biomarkers meeting a significance threshold of -log(10) q-value >10 are shown as stacked bar graphs separated by NP formulation and time point. PEGylated NP formulations are highlighted with a gray background. (**C**) A heatmap showing all gene- and protein- expression features with positive correlation identified by random forest algorithm in columns, and NP formulations in rows. Features are colored based on their Pearson correlation and clustered using k-means clustering, with clusters 1+2 highlighted as features present across multiple NP formulations. (**D**) Visual representation of the STRING network generated by inputting the 205 features from clusters 1+2, with network statistics. Each node represents a feature, and the edges represent predicted functional associations. The most interconnected nodes are labeled in the zoomed inset.

Biomarker number and significance are influenced by nanoparticle properties

We employed univariate analysis to correlate association and CCLE features for each NP formulation, thresholding q-values less than $1x10^{-10}$ (Figure 2B). Selection of this cutoff was guided by the IgG-conjugated antibody analysis, which returned few hits above this threshold. For liposomal NPs, we observed that the number of significant biomarkers was higher at 4 h than 24 h. We believe this may be indicative of active uptake processes, established to take place within the first few hours of NP-cell interactions, whereas at 24 hours, we may be capturing features associated with less specific interactions.[37, 38] We also observed that liposome surface modification influences the number and significance of biomarkers. Specifically, liposomes electrostatically coated with polysaccharides (HA, ALG, DXS, FUC, CS) had the highest amount of associated biomarkers, which we hypothesize is due to the high degree of interactions between sugars and cell surface proteins as well as the potential for naturally occurring polysaccharides to interact with a wide range of cell surface elements.[24, 39, 40] In line with this hypothesis, the addition of PEG, a well-established antifouling polymer, reduces the number and significance of associated biomarkers almost to zero. In contrast to the highly specific hits generated from EGFR-conjugated liposomes (formulated using 25% PEG liposomes), this abrupt decrease in significant biomarkers further indicates the ability of our platform to identify specific NP binding and recognition elements. In contrast to the liposomal formulations, PLGA formulations, regardless of surface modification, resulted in few biomarkers at either time point. Lastly, a high number of significant biomarkers was associated with both carboxylated and sulfated PS NPs included in our screen, though there was no time dependence, in contrast to the liposomal formulation. While this result was initially surprising, as the PS formulations are made of synthetic polystyrene polymers, meaningful biological interactions with anionic polystyrenes, both in polymer and particle form, have been reported.[41] Specifically, it was described that these systems have the appropriate mix of hydrophobicity and anionic charge character to interact favorably with trafficking proteins, including the caveolins.

NP biomarkers are connected and create trafficking networks

We additionally identified predictive biomarkers for the tested NP formulations using a random-forest algorithm (methods in Supplementary Text). We narrowed these hits to include the categories of gene expression, gene copy number, or protein abundance. Data from the 4 h time point was chosen for this analysis based on the EGFR-related hits for liposomes, which were more significant at 4 h than at 24 h. As we were interested in applying this approach to identify cellular features positively correlated with uptake (e.g., increased expression of trafficking proteins), hits negatively correlated with NP association were removed from this analysis. Next, we used K-means clustering to visualize biomarkers based on their relative importance and presence across formulations (Figure 2C). Clusters 1 and 2 contained many hits shared across NP formulations and were especially enriched for liposomal and PS NPs. These 205 genes and proteins were input into the STRING database[42-44] to generate a protein-protein interaction (PPI) network that was found to be highly interconnected (PPI enrichment p-value $<1x10^{-16}$) (Figure 2D). Notably, the network is enriched in proteins found in the plasma membrane, extracellular region, and extracellular matrix (false discovery rate [FDR] = $8x10^{-12}$, $3x10^{-9}$, and $3x10^{-8}$, respectively) based on enrichment analysis with gene ontology (GO) localization datasets (Figure S8).[45-47] The identification of overlapping biomarkers that are localized to the cell surface and have established protein-protein interactions led us to hypothesize that these proteins are important in early NP trafficking. Enrichment analyses using GO molecular functions datasets showed enrichment in numerous binding processes

(Data S1, Figure S8), giving further credence to this theory. These results serve as a framework for the comprehensive investigation of cellular processes important for NP engagement, which may prove useful for fundamental trafficking studies and target identification.

SLC46A3 is a strongly predictive biomarker for liposomal nanoparticle uptake

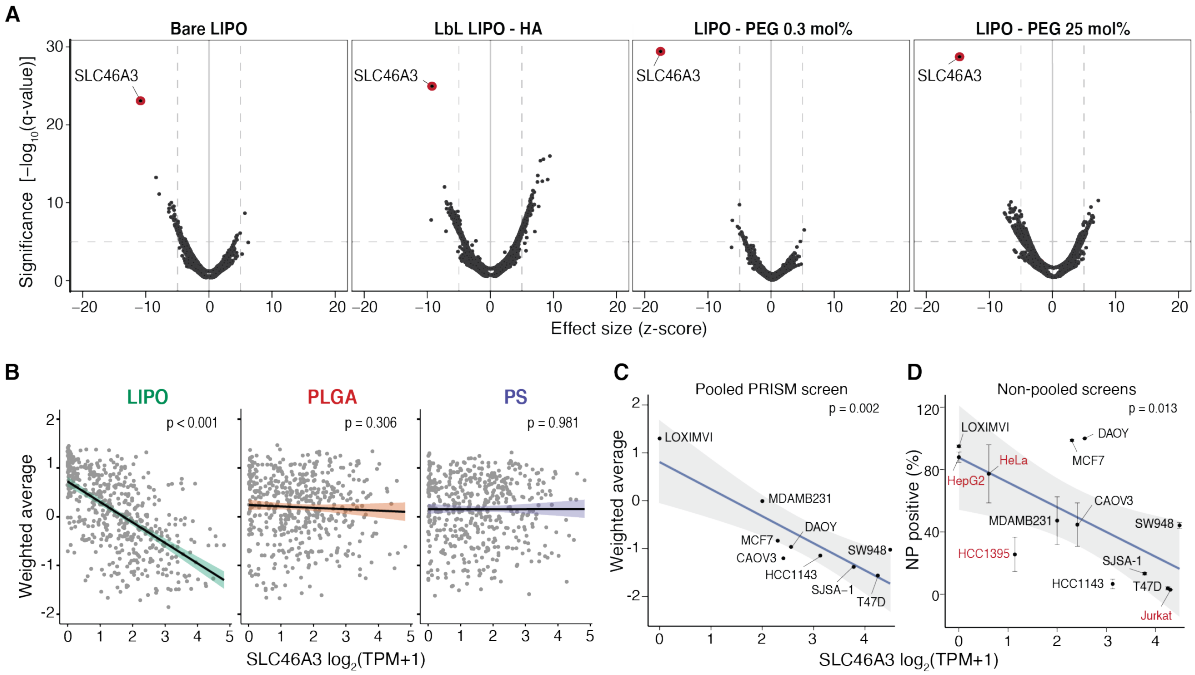

Figure 3. Native expression of the lysosomal transporter SLC46A3 is strongly predictive of NP-cell interaction for liposome formulations. (**A**) Univariate analysis identifies SLC46A3 expression as strongly yet inversely correlated with liposome association, regardless of liposomal surface modification. (**B**) Using linear regression to evaluate the biomarker relationship across core formulations reveals *SLC46A3* expression is inversely correlated with NP association in liposome-cell line pairs ($p < 0.001$) but not PLGA- and PS-cell line pairs ($p > 0.05$); n=488 for each plot. (**C**) Cell lines in the nanoPRISM pool exhibit a range of natural *SLC46A3* expression levels with a log linear correlation with uptake of liposomes. (**D**) This correlation is also exhibited when assessing liposome-cell associations via flow cytometry in a non-pooled fashion ($p = 0.013$). Cell lines in red were not part of the pooled PRISM screen. Data represented in D is shown as the mean and standard deviation of four biological replicates.

Evaluating univariate results across NP formulations, we identified one biomarker with a strong, inverse relationship with liposomal NP association: expression of solute carrier family 46 member 3 (*SLC46A3*), a lysosomal transporter. SLC46A3 has been implicated in the metabolism of antibody-drug conjugates,[48-50] but this is, to our knowledge, the first description of SLC46A3 as a NP-specific biomarker. Moreover, downregulation of SLC46A3 has been reported to play a role in cancer cell malignancy and therapy resistance in several cancers.[51, 52] Given these significant therapeutic implications, we sought to validate the predictive power of *SLC46A3* expression for liposomal NP association.

SLC46A3 expression was the most significant hit on univariate analysis and also the top ranked random forest feature for each liposomal NP tested at 24 h, regardless of surface

modification (Figures 3A and S9A, B). This inverse relationship between *SLC46A3* expression and NP association was found to be specific to liposomal NPs, and not observed with PLGA or PS NPs (Figures 3B and S9A).

We selected nine cancer cell lines (CAOV3, DAOY, HCC1143, LOXIMVI, MCF7, MDAMB231, SJSA-1, SW948, T47D) from the nanoPRISM pool with a range of native *SLC46A3* expression levels for screening in a non-pooled fashion (Figure 3C). Analogous to the pooled screen, individual cell lines were profiled using flow cytometry and NP-associated fluorescence was quantified after 24 h incubation (Figures 3D and S10, S11). In line with observations from pooled screening, the inverse relationship between liposome association and native *SLC46A3* expression was maintained, suggesting that *SLC46A3* may play a key role in trafficking of liposomal NPs.

We further selected four cell lines (HeLa, HepG2, HCC1395, Jurkat) that were not included in the PRISM pools with a range of native *SLC46A3* expression levels to profile for liposomal NP association. We found that liposomal NP association again inversely correlated with *SLC46A3* expression levels, recapitulating the *SLC46A3*-dependent trend observed in PRISM cells (Figure 3D).

SLC46A3 expression regulates liposomal nanoparticle uptake

We selected two cancer cell lines from the pooled screen to further functionally probe whether SLC46A3 expression level governs NP association: LOXIMVI, with low native expression, and T47D, with high native expression (Figure 4A). These cell lines displayed a strong phenotype in the pooled screen, with LOXIMVI having high association and T47D having low association with liposomal NP formulations (Figure 4B).

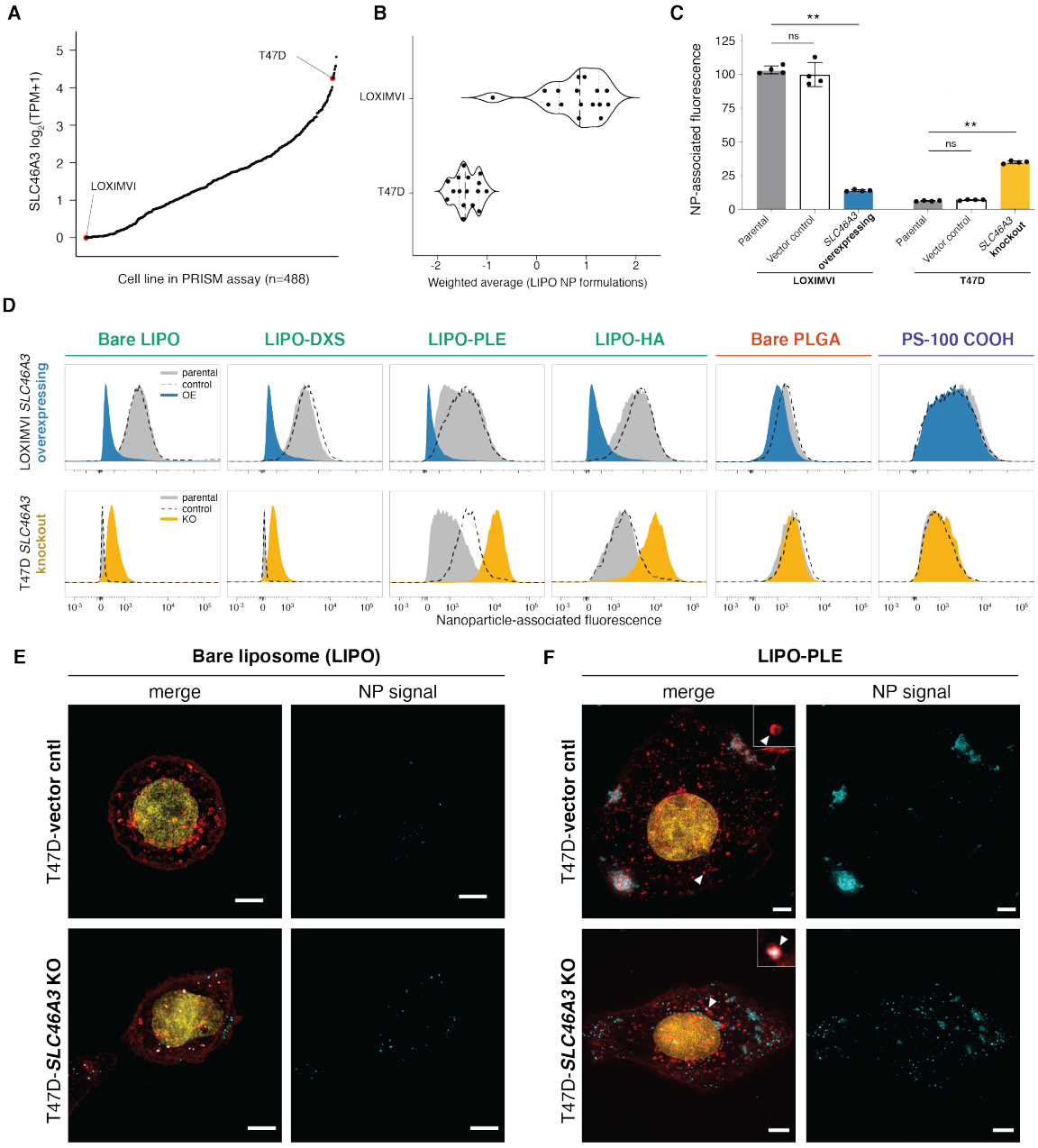

Figure 4. Modulating *SLC46A3* expression in cancer cell lines is sufficient to regulate strength of interaction with liposome NP formulations. (**A**) T47D and LOXIMVI cells have high and low *SLC46A3* expression, respectively, with respect to *SLC46A3* expression levels represented in the nanoPRISM cell line pool. (**B**) LOXIMVI cells have predominantly high association with all tested liposomal NP formulations and T47D cells have low association with all tested liposomal NP formulations. (**C**) Using lentivirus to overexpress *SLC46A3* in LOXIMVI cells and CRISPR/Cas9 to knock out *SLC46A3* in T47D cells, we show that modulation results in significantly changed liposome association, as determined via flow cytometry (** $p < 0.001$, Kruskal-Wallis test), NP-associated fluorescence is defined as median fluorescence intensity normalized to untreated cells. (**D**) These shifts in NP association were consistently observed across all tested liposomes, independent of surface modification. No shifts were observed with PLGA or PS formulations. Representative optical microscopy images of engineered T47D cells treated with

(**E**) liposomal and (**F**) Lipo-PLE NPs for 24 h revealed changed subcellular trafficking in the T47D-*SLC46A3* KO line with increased intracellular uptake. Wheat germ agglutinin (red) was used to stain cell membranes (cyan = NPs, yellow = nuclei). Scale bar = 5 μm.

First, we performed lentiviral vector overexpression of SLC46A3 or luciferase (vector control) in LOXIMVI cells (Figure S12). Overexpression of SLC46A3 in LOXIMVI cells significantly abrogated interaction with bare liposomes (p = 0.006) using flow cytometry profiling (Figure 4C). Next, we employed the CRISPR/Cas9 system with single guide RNA directed against *SLC46A3* or GFP (vector control) in T47D cells and generated clonal knockout cell lines (Figures S13). The T47D-*SLC46A3* knockout cell line demonstrated significantly increased association with bare liposomes compared to parental or vector control lines (p 0.0017, Figure 4C). We also confirmed that the presence of serum proteins in cell culture media does not abrogate this trend (Figure S14). Taken together, these data indicate modulation of SLC46A3 alone in cancer cells is sufficient to predictably govern association and uptake of an unmodified liposome.

To expand on these results, we further tested our engineered cell lines with a subset of our NP library, including surface functionalized liposomes as well as PLGA and PS NPs. In line with our prior observations, association of all tested liposomal NPs was inverse to SLC46A3 expression (Figure 4D). Moreover, no significant changes in NP association were observed for PLGA and PS NPs, further validating the specificity of SLC46A3 as a liposomal biomarker.

We utilized optical microscopy to investigate the impact of SLC46A3 on subcellular trafficking of liposomal NPs (Figure 4E). In agreement with the flow cytometry results, we saw minimal internalization of liposomal NPs in T47D vector control cells. In contrast, T47D-SLC46A3 knockout cells took up larger amounts of liposomes, which appear to localize in vesicles near the cell membrane (Figure 4E, bottom panels).

As SLC46A3 has been implicated in transmembrane trafficking,[48-50] we sought to investigate how modulating expression might affect NPs with established cell surface localization. To this end, we selected liposomes electrostatically coated with poly-L-glutamate (Lipo-PLE), which we have previously established to remain extracellularly associated on a number of ovarian cancer cell lines, for further study.[9, 53] In agreement with our prior findings, we observed that Lipo-PLE NPs remain predominantly extracellularly associated with the T47D vector control cells (Figure 4F, upper panels). However, we observed a stark difference in Lipo-PLE trafficking in the T47D-SLC46A3 knockout cells, where in addition to some extracellular association, a significant portion of particles appear to be internalized in vesicles distributed uniformly throughout the cytoplasm (Figure 4F, bottom panels).

Discussion and Conclusions

This work represents the first high-throughput interrogation of NP-cancer cell interactions through the lens of multi-omics. Harnessing the power of pooled screening and high throughput sequencing, we developed and validated a platform to identify predictive biomarkers for NP interactions with cancer cells. We utilized this platform to screen a 35 member NP library against a panel of 488 cancer cell lines. This enabled the comprehensive study and identification of key parameters mediating NP-cell interactions, highlighting the importance of considering both nanomaterials and cellular features in concert.

Moreover, through the use of univariate analyses and random forest algorithms, we identified biomarkers correlated with NP association. The robust and quantitative nature with which we detected EGFR hits for antibody-targeted NPs shows the utility of this platform for the development and optimization of antibody-targeted therapeutics.

By clustering NP-specific biomarkers across formulations, we constructed interaction networks, identifying and connecting genes associated with NP binding, recognition, and subcellular trafficking. This provides the scientific community with a blueprint for the fundamental study of cellular processes mediating NP engagement, with applications for both basic and translational research.

We additionally identified gene expression of *SLC46A3* as a strongly predictive biomarker of liposomal NP uptake. We first validated these findings in a panel of non-pooled cell lines, followed by engineered cell lines with modulated *SLC46A3* levels. Importantly, as all current FDA approved NPs for anticancer applications are liposomal formulations, there is significant potential for this biomarker to be quickly implemented in clinical studies with existing, approved formulations. Our *in vitro* findings present the key first step toward identifying and utilizing such NP-specific biomarkers.

In summary, we present a powerful platform to study NP-cancer cell interactions simultaneously through the use of pooled screening, genomics, and machine learning algorithms. This provides a new dimension to the study of cancer nanomedicine. Application of this platform will serve useful not only for the rational design of nanocarriers, but also for the identification of specific phenotypes primed to benefit from targeted drug delivery and nanomedicine.

References

1. Shi, J. J.; Kantoff, P. W.; Wooster, R.; Farokhzad, O. C., Cancer nanomedicine: progress, challenges and opportunities. *Nat. Rev. Cancer* **2017,** *17* (1), 20-37.
2. Mitchell, M. J.; Billingsley, M. M.; Haley, R. M.; Wechsler, M. E.; Peppas, N. A.; Langer, R., Engineering precision nanoparticles for drug delivery. *Nat. Rev. Drug. Discov.* **2020**, *20*, 101-124.
3. Tran, S.; DeGiovanni, P. J.; Piel, B.; Rai, P., Cancer nanomedicine: a review of recent success in drug delivery. *Clin Transl Med* **2017,** *6* (1), 1-21.
4. Wilhelm, S.; Tavares, A. J.; Dai, Q.; Ohta, S.; Audet, J.; Dvorak, H. F.; Chan, W. C. W., Analysis of nanoparticle delivery to tumours. *Nat. Rev. Mater.* **2016,** *1* (5), 16014.
5. Cheng, Y. H.; He, C. L.; Riviere, J. E.; Monteiro-Riviere, N. A.; Lin, Z. M., Meta-Analysis of Nanoparticle Delivery to Tumors Using a Physiologically Based Pharmacokinetic Modeling and Simulation Approach. *ACS Nano* **2020,** *14* (3), 3075-3095.
6. Youn, Y. S.; Bae, Y. H., Perspectives on the past, present, and future of cancer nanomedicine. *Adv. Drug Deliver. Rev.* **2018,** *130*, 3-11.
7. Poon, W.; Kingston, B. R.; Ouyang, B.; Ngo, W.; Chan, W. C. W., A framework for designing delivery systems. *Nat. Nanotechnol.* **2020,** *15* (10), 819-829.
8. Poon, W.; Zhang, Y. N.; Ouyang, B.; Kingston, B. R.; Wu, J. L. Y.; Wilhelm, S.; Chan, W. C. W., Elimination Pathways of Nanoparticles. *ACS Nano* **2019,** *13* (5), 5785-5798.
9. Correa, S.; Boehnke, N.; Barberio, A. E.; Deiss-Yehiely, E.; Shi, A.; Oberlton, B.; Smith, S. G.; Zervantonakis, I.; Dreaden, E. C.; Hammond, P. T., Tuning Nanoparticle Interactions with Ovarian Cancer through Layer-by-Layer Modification of Surface Chemistry. *ACS Nano* **2020,** *14* (2), 2224-2237.
10. Boehnke, N.; Correa, S.; Hao, L.; Wang, W.; Straehla, J. P.; Bhatia, S. N.; Hammond, P. T., Theranostic Layer-by-Layer Nanoparticles for Simultaneous Tumor Detection and Gene Silencing. *Angew. Chem. Int. Ed. Engl.* **2020,** *59* (7), 2776-2783.
11. Boehnke, N.; Dolph, K. J.; Juarez, V. M.; Lanoha, J. M.; Hammond, P. T., Electrostatic Conjugation of Nanoparticle Surfaces with Functional Peptide Motifs. *Bioconjug. Chem.* **2020,** *31* (9), 2211-2219.
12. Dahlman, J. E.; Kauffman, K. J.; Xing, Y. P.; Shaw, T. E.; Mir, F. F.; Dlott, C. C.; Langer, R.; Anderson, D. G.; Wang, E. T., Barcoded nanoparticles for high throughput in vivo discovery of targeted therapeutics. *Proc. Natl. Acad. Sci. USA* **2017,** *114* (8), 2060-2065.
13. Kenry; Yeo, T.; Manghnani, P. N.; Middha, E.; Pan, Y. T.; Chen, H.; Lim, C. T.; Liu, B., Mechanistic Understanding of the Biological Responses to Polymeric Nanoparticles. *ACS Nano* **2020,** *14* (4), 4509-4522.
14. Shamay, Y.; Shah, J.; Isik, M.; Mizrachi, A.; Leibold, J.; Tschaharganeh, D. F.; Roxbury, D.; Budhathoki-Uprety, J.; Nawaly, K.; Sugarman, J. L.; Baut, E.; Neiman, M. R.; Dacek, M.; Ganesh, K. S.; Johnson, D. C.; Sridharan, R.; Chu, K. L.; Rajasekhar, V. K.; Lowe, S. W.; Chodera, J. D.; Heller, D. A., Quantitative self-assembly prediction yields targeted nanomedicines. *Nat. Mater.* **2018,** *17* (4), 361-368.
15. Nogrady, B., How cancer genomics is transforming diagnosis and treatment. *Nature* **2020,** *579* (7800), S10-S11.
16. Yu, C. N.; Mannan, A. M.; Yvone, G. M.; Ross, K. N.; Zhang, Y. L.; Marton, M. A.; Taylor, B. R.; Crenshaw, A.; Gould, J. Z.; Tamayo, P.; Weir, B. A.; Tsherniak, A.; Wong, B.; Garraway, L. A.; Shamji, A. F.; Palmer, M. A.; Foley, M. A.; Winckler, W.; Schreiber, S. L.; Kung, A. L.; Golub, T. R., High-throughput identification of genotype-specific cancer vulnerabilities in mixtures of barcoded tumor cell lines. *Nat. Biotechnol.* **2016,** *34* (4), 419-423.

17. Corsello, S. M.; Nagari, R. T.; Spangler, R. D.; Rossen, J.; Kocak, M.; Bryan, J. G.; Humeidi, R.; Peck, D.; Wu, X.; Tang, A. A.; Wang, V. M.; Bender, S.; Lemire, E.; Narayan, R.; Montgomery, P.; Ben-David, U.; Garvie, C. W.; Chen, Y.; Rees, M. G.; Lyons, N. J.; McFarland, J. M.; Wong, B. T.; Wang, L.; Dumont, N.; O'Hearn, P. J.; Stefan, E. J.; Doench, J. G.; Harrington, C.; Greulich, H.; Meyerson, M.; Vazquez, F.; Subramaniam, A.; Roth, J. A.; Bittker, J. A.; Boehm, J. S.; Mader, C. C.; Tsherniak, A.; Golub, T. R., Discovering the anticancer potential of non-oncology drugs by systematic viability profiling. *Nat. Cancer* **2020,** *1*, 235-248.
18. Correa, S.; Boehnke, N.; Deiss-Yehiely, E.; Hammond, P. T., Solution Conditions Tune and Optimize Loading of Therapeutic Polyelectrolytes into Layer-by-Layer Functionalized Liposomes. *ACS Nano* **2019,** *13* (5), 5623-5634.
19. Correa, S.; Choi, K. Y.; Dreaden, E. C.; Renggli, K.; Shi, A.; Gu, L.; Shopsowitz, K. E.; Quadir, M. A.; Ben-Akiva, E.; Hammond, P. T., Highly Scalable, Closed-Loop Synthesis of Drug-Loaded, Layer-by-Layer Nanoparticles. *Adv. Funct. Mater.* **2016,** *26* (7), 991-1003.
20. Deng, Z. J.; Morton, S. W.; Ben-Akiva, E.; Dreaden, E. C.; Shopsowitz, K. E.; Hammond, P. T., Layer-by-Layer Nanoparticles for Systemic Codelivery of an Anticancer Drug and siRNA for Potential Triple-Negative Breast Cancer Treatment. *ACS Nano* **2013,** *7* (11), 9571-9584.
21. Morton, S. W.; Poon, Z. Y.; Hammond, P. T., The architecture and biological performance of drug-loaded LbL nanoparticles. *Biomaterials* **2013,** *34* (21), 5328-5335.
22. Decher, G., Fuzzy nanoassemblies: Toward layered polymeric multicomposites. *Science* **1997,** *277* (5330), 1232-1237.
23. Dreaden, E. C.; Kong, Y. W.; Morton, S. W.; Correa, S.; Choi, K. Y.; Shopsowitz, K. E.; Renggli, K.; Drapkin, R.; Yaffe, M. B.; Hammond, P. T., Tumor-Targeted Synergistic Blockade of MAPK and PI3K from a Layer-by-Layer Nanoparticle. *Clin. Cancer Res.* **2015,** *21* (19), 4410-4419.
24. Dreaden, E. C.; Morton, S. W.; Shopsowitz, K. E.; Choi, J. H.; Deng, Z. J.; Cho, N. J.; Hammond, P. T., Bimodal Tumor-Targeting from Microenvironment Responsive Hyaluronan Layer-by-Layer (LbL) Nanoparticles. *ACS Nano* **2014,** *8* (8), 8374-8382.
25. Oommen, O. P.; Duehrkop, C.; Nilsson, B.; Hilborn, J.; Varghese, O. P., Multifunctional Hyaluronic Acid and Chondroitin Sulfate Nanoparticles: Impact of Glycosaminoglycan Presentation on Receptor Mediated Cellular Uptake and Immune Activation. *ACS Appl. Mater. Inter.* **2016,** *8* (32), 20614-20624.
26. Suk, J. S.; Xu, Q. G.; Kim, N.; Hanes, J.; Ensign, L. M., PEGylation as a strategy for improving nanoparticle-based drug and gene delivery. *Adv. Drug Deliver. Rev.* **2016,** *99*, 28-51.
27. Frohlich, E., The role of surface charge in cellular uptake and cytotoxicity of medical nanoparticles. *Int. J. Nanomed.* **2012,** *7*, 5577-5591.
28. Berg, E. A.; Fishman, J. B., Labeling Antibodies Using N-Hydroxysuccinimide (NHS)-Fluorescein. *Cold Spring Harb. Protoc.* **2019,** *3*, 229-231.
29. Jin, X.; Demere, Z.; Nair, K.; Ali, A.; Ferraro, G. B.; Natoli, T.; Deik, A.; Petronio, L.; Tang, A. A.; Zhu, C.; Wang, L.; Rosenberg, D.; Mangena, V.; Roth, J.; Chung, K.; Jain, R. K.; Clish, C. B.; Heiden, M. G. V.; Golub, T. R., A metastasis map of human cancer cell lines. *Nature* **2020,** *588* (7837), 331-36.
30. Kim, J. A.; Aberg, C.; Salvati, A.; Dawson, K. A., Role of cell cycle on the cellular uptake and dilution of nanoparticles in a cell population. *Nat. Nanotechnol.* **2012,** *7* (1), 62-68.
31. Aberg, C.; Kim, J. A.; Salvati, A.; Dawson, K. A., Reply to 'The interface of nanoparticles with proliferating mammalian cells'. *Nat. Nanotechnol.* **2017,** *12* (7), 600-603.

32. Panet, E.; Mashriki, T.; Lahmi, R.; Jacob, A.; Ozer, E.; Vecsler, M.; Lazar, I.; Tzur, A., The interface of nanoparticles with proliferating mammalian cells. *Nat. Nanotechnol.* **2017,** *12* (7), 598-600.
33. Rees, P.; Wills, J. W.; Brown, M. R.; Barnes, C. M.; Summers, H. D., The origin of heterogeneous nanoparticle uptake by cells. *Nat. Commun.* **2019,** *10*.
34. Barretina, J.; Caponigro, G.; Stransky, N.; Venkatesan, K.; Margolin, A. A.; Kim, S.; Wilson, C. J.; Lehar, J.; Kryukov, G. V.; Sonkin, D.; Reddy, A.; Liu, M.; Murray, L.; Berger, M. F.; Monahan, J. E.; Morais, P.; Meltzer, J.; Korejwa, A.; Jane-Valbuena, J.; Mapa, F. A.; Thibault, J.; Bric-Furlong, E.; Raman, P.; Shipway, A.; Engels, I. H.; Cheng, J.; Yu, G. K.; Yu, J. J.; Aspesi, P.; de Silva, M.; Jagtap, K.; Jones, M. D.; Wang, L.; Hatton, C.; Palescandolo, E.; Gupta, S.; Mahan, S.; Sougnez, C.; Onofrio, R. C.; Liefeld, T.; MacConaill, L.; Winckler, W.; Reich, M.; Li, N. X.; Mesirov, J. P.; Gabriel, S. B.; Getz, G.; Ardlie, K.; Chan, V.; Myer, V. E.; Weber, B. L.; Porter, J.; Warmuth, M.; Finan, P.; Harris, J. L.; Meyerson, M.; Golub, T. R.; Morrissey, M. P.; Sellers, W. R.; Schlegel, R.; Garraway, L. A., The Cancer Cell Line Encyclopedia enables predictive modelling of anticancer drug sensitivity. *Nature* **2012,** *483*, 603-607.
35. Ghandi, M.; Huang, F. W.; Jane-Valbuena, J.; Kryukov, G. V.; Lo, C. C.; McDonald, E. R.; Barretina, J.; Gelfand, E. T.; Bielski, C. M.; Li, H.; Hu, K.; Andreev-Drakhlin, A. Y.; Kim, J.; Hess, J. M.; Haas, B. J.; Aguet, F.; Weir, B. A.; Rothberg, M. V.; Paolella, B. R.; Lawrence, M. S.; Akbani, R.; Lu, Y.; Tiv, H. L.; Gokhale, P. C.; De Weck, A.; Mansour, A. A.; Oh, C.; Shih, J.; Hadi, K.; Rosen, Y.; Bistline, J.; Venkatesan, K.; Reddy, A.; Sonkin, D.; Liu, M.; Lehar, J.; Korn, J. M.; Porter, D. A.; Jones, M. D.; Golji, J.; Caponigro, G.; Taylor, J. E.; Dunning, C. M.; Creech, A. L.; Warren, A. C.; McFarland, J. M.; Zamanighomi, M.; Kauffmann, A.; Stransky, N.; Imielinski, M.; Maruvka, Y. E.; Cherniack, A. D.; Tsherniak, A.; Vazquez, F.; Jaffe, J. D.; Lane, A. A.; Weinstock, D. M.; Johannessen, C. M.; Morrissey, M. P.; Stegmeier, F.; Schlegel, R.; Hahn, W. C.; Getz, G.; Mills, G. B.; Boehm, J. S.; Golub, T. R.; Garraway, L. A.; Sellers, W. R., Next-generation characterization of the Cancer Cell Line Encyclopedia. *Nature* **2019,** *569* (7757), 503-508.
36. Tsuchikama, K.; An, Z. Q., Antibody-drug conjugates: recent advances in conjugation and linker chemistries. *Protein Cell* **2018,** *9* (1), 33-46.
37. Rejman, J.; Oberle, V.; Zuhorn, I. S.; Hoekstra, D., Size-dependent internalization of particles via the pathways of clathrin-and caveolae-mediated endocytosis. *Biochem. J.* **2004,** *377*, 159-169.
38. Behzadi, S.; Serpooshan, V.; Tao, W.; Hamaly, M. A.; Alkawareek, M. Y.; Dreaden, E. C.; Brown, D.; Alkilany, A. M.; Farokhzad, O. C.; Mahmoudi, M., Cellular uptake of nanoparticles: journey inside the cell. *Chem. Soc. Rev.* **2017,** *46* (14), 4218-4244.
39. Shamay, Y.; Elkabets, M.; Li, H.; Shah, J.; Brook, S.; Wang, F.; Adler, K.; Baut, E.; Scaltriti, M.; Jena, P. V.; Gardner, E. E.; Poirier, J. T.; Rudin, C. M.; Baselga, J.; Haimovitz-Friedman, A.; Heller, D. A., P-selectin is a nanotherapeutic delivery target in the tumor microenvironment. *Sci. Transl. Med.* **2018,** *8* (345), 345ra87.
40. Saravanakumar, G.; Jo, D. G.; Park, J. H., Polysaccharide-Based Nanoparticles: A Versatile Platform for Drug Delivery and Biomedical Imaging. *Curr. Med. Chem.* **2012,** *19* (19), 3212-3229.
41. Voigt, J.; Christensen, J.; Shastri, V. P., Differential uptake of nanoparticles by endothelial cells through polyelectrolytes with affinity for caveolae. *Proc. Natl. Acad. Sci. USA* **2014,** *111* (8), 2942-2947.
42. Szklarczyk, D.; Gable, A. L.; Lyon, D.; Junge, A.; Wyder, S.; Huerta-Cepas, J.; Simonovic, M.; Doncheva, N. T.; Morris, J. H.; Bork, P.; Jensen, L. J.; Mering, C., STRING

v11: protein-protein association networks with increased coverage, supporting functional discovery in genome-wide experimental datasets. *Nucleic Acids Res.* **2019,** *47* (D1), D607-D613.
43. von Mering, C.; Huynen, M.; Jaeggi, D.; Schmidt, S.; Bork, P.; Snel, B., STRING: a database of predicted functional associations between proteins. *Nucleic Acids Res.* **2003,** *31* (1), 258-261.
44. Snel, B.; Lehmann, G.; Bork, P.; Huynen, M. A., STRING: a web-server to retrieve and display the repeatedly occurring neighbourhood of a gene. *Nucleic Acids Res.* **2000,** *28* (18), 3442-3444.
45. Martin, D.; Brun, C.; Remy, E.; Mouren, P.; Thieffry, D.; Jacq, B., GOToolBox: functional analysis of gene datasets based on Gene Ontology. *Genome Biol.* **2004,** *5* (12), R101.
46. Ashburner, M.; Ball, C. A.; Blake, J. A.; Botstein, D.; Butler, H.; Cherry, J. M.; Davis, A. P.; Dolinski, K.; Dwight, S. S.; Eppig, J. T.; Harris, M. A.; Hill, D. P.; Issel-Tarver, L.; Kasarskis, A.; Lewis, S.; Matese, J. C.; Richardson, J. E.; Ringwald, M.; Rubin, G. M.; Sherlock, G.; Consortium, G. O., Gene Ontology: tool for the unification of biology. *Nat. Genet/* **2000,** *25* (1), 25-29.
47. Carbon, S.; Douglass, E.; Good, B. M.; Unni, D. R.; Harris, N. L.; Mungall, C. J.; Basu, S.; Chisholm, R. L.; Dodson, R. J.; Hartline, E.; Fey, P.; Thomas, P. D.; Albou, L. P.; Ebert, D.; Kesling, M. J.; Mi, H. Y.; Muruganujan, A.; Huang, X. S.; Mushayahama, T.; LaBonte, S. A.; Siegele, D. A.; Antonazzo, G.; Attrill, H.; Brown, N. H.; Garapati, P.; Marygold, S. J.; Trovisco, V.; Dos Santos, G.; Falls, K.; Tabone, C.; Zhou, P. L.; Goodman, J. L.; Strelets, V. B.; Thurmond, J.; Garmiri, P.; Ishtiaq, R.; Rodriguez-Lopez, M.; Acencio, M. L.; Kuiper, M.; Laegreid, A.; Logie, C.; Lovering, R. C.; Kramarz, B.; Saverimuttu, S. C. C.; Pinheiro, S. M.; Gunn, H.; Su, R. Z.; Thurlow, K. E.; Chibucos, M.; Giglio, M.; Nadendla, S.; Munro, J.; Jackson, R.; Duesbury, M. J.; Del-Toro, N.; Meldal, B. H. M.; Paneerselvam, K.; Perfetto, L.; Porras, P.; Orchard, S.; Shrivastava, A.; Chang, H. Y.; Finn, R. D.; Mitchell, A. L.; Rawlings, N. D.; Richardson, L.; Sangrador-Vegas, A.; Blake, J. A.; Christie, K. R.; Dolan, M. E.; Drabkin, H. J.; Hill, D. P.; Ni, L.; Sitnikov, D. M.; Harris, M. A.; Oliver, S. G.; Rutherford, K.; Wood, V.; Hayles, J.; Bahler, J.; Bolton, E. R.; De Pons, J. L.; Dwinell, M. R.; Hayman, G. T.; Kaldunski, M. L.; Kwitek, A. E.; Laulederkind, S. J. F.; Plasterer, C.; Tutaj, M. A.; Vedi, M.; Wang, S. J.; D'Eustachio, P.; Matthews, L.; Balhoff, J. P.; Aleksander, S. A.; Alexander, M. J.; Cherry, J. M.; Engel, S. R.; Gondwe, F.; Karra, K.; Miyasato, S. R.; Nash, R. S.; Simison, M.; Skrzypek, M. S.; Weng, S.; Wong, E. D.; Feuermann, M.; Gaudet, P.; Morgat, A.; Bakker, E.; Berardini, T. Z.; Reiser, L.; Subramaniam, S.; Huala, E.; Arighi, C. N.; Auchincloss, A.; Axelsen, K.; Argoud-Puy, G.; Bateman, A.; Blatter, M. C.; Boutet, E.; Bowler, E.; Breuza, L.; Bridge, A.; Britto, R.; Bye-A-Jee, H.; Casas, C. C.; Coudert, E.; Denny, P.; Estreicher, A.; Famiglietti, M. L.; Georghiou, G.; Gos, A.; Gruaz-Gumowski, N.; Hatton-Ellis, E.; Hulo, C.; Ignatchenko, A.; Jungo, F.; Laiho, K.; Le Mercier, P.; Lieberherr, D.; Lock, A.; Lussi, Y.; MacDougall, A.; Magrane, M.; Martin, M. J.; Masson, P.; Natale, D. A.; Hyka-Nouspikel, N.; Orchard, S.; Pedruzzi, I.; Pourcel, L.; Poux, S.; Pundir, S.; Rivoire, C.; Speretta, E.; Sundaram, S.; Tyagi, N.; Warner, K.; Zaru, R.; Wu, C. H.; Diehl, A. D.; Chan, J. N.; Grove, C.; Lee, R. Y. N.; Muller, H. M.; Raciti, D.; Van Auken, K.; Sternberg, P. W.; Berriman, M.; Paulini, M.; Howe, K.; Gao, S.; Wright, A.; Stein, L.; Howe, D. G.; Toro, S.; Westerfield, M.; Jaiswal, P.; Cooper, L.; Elser, J.; Consortium, G. O., The Gene Ontology resource: enriching a GOld mine. *Nucleic Acids Res.* **2021,** *49* (D1), D325-D334.
48. Hamblett, K. J.; Jacob, A. P.; Gurgel, J. L.; Tometsko, M. E.; Rock, B. M.; Patel, S. K.; Milburn, R. R.; Siu, S.; Ragan, S. P.; Rock, D. A.; Borths, C. J.; O'Neill, J. W.; Chang, W. S.; Weidner, M. F.; Bio, M. M.; Quon, K. C.; Fanslow, W. C., SLC46A3 Is Required to

Transport Catabolites of Noncleavable Antibody Maytansine Conjugates from the Lysosome to the Cytoplasm. *Cancer Res.* **2015,** *75* (24), 5329-5340.
49. Tsui, C. K.; Barfield, R. M.; Fischer, C. R.; Morgens, D. W.; Li, A.; Smith, B. A. H.; Gray, M. A.; Bertozzi, C. R.; Rabuka, D.; Bassik, M. C., CRISPR-Cas9 screens identify regulators of antibody-drug conjugate toxicity. *Nat. Chem. Biol.* **2019,** *15* (10), 949-958.
50. Kinneer, K.; Meekin, J.; Tiberghien, A. C.; Tai, Y. T.; Phipps, S.; Kiefer, C. M.; Rebelatto, M. C.; Dimasi, N.; Moriarty, A.; Papadopoulos, K. P.; Sridhar, S.; Gregson, S. J.; Wick, M. J.; Masterson, L.; Anderson, K. C.; Herbst, R.; Howard, P. W.; Tice, D. A., SLC46A3 as a Potential Predictive Biomarker for Antibody-Drug Conjugates Bearing Noncleavable Linked Maytansinoid and Pyrrolobenzodiazepine Warheads. *Clin. Cancer Res.* **2018,** *24* (24), 6570-6582.
51. Zhao, Q.; Zheng, B.; Meng, S. Q.; Xu, Y.; Guo, J.; Chen, L. J.; Xiao, J.; Zhang, W.; Tan, Z. R.; Tang, J.; Chen, L.; Chen, Y., Increased expression of SLC46A3 to oppose the progression of hepatocellular carcinoma and its effect on sorafenib therapy. *Biomed. Pharmacother.* **2019,** *114,* 108864.
52. Li, G. M.; Guo, J.; Shen, B. Q.; Yadav, D. B.; Sliwkowski, M. X.; Crocker, L. M.; Lacap, J. A.; Phillips, G. D. L., Mechanisms of Acquired Resistance to Trastuzumab Emtansine in Breast Cancer Cells. *Mol. Cancer Ther.* **2018,** *17* (7), 1441-1453.
53. Barberio, A. E.; Smith, S. G.; Correa, S.; Nguyen, C.; Nhan, B.; Melo, M.; Tokatlian, T.; Suh, H.; Irvine, D. J.; Hammond, P. T., Cancer Cell Coating Nanoparticles for Optimal Tumor-Specific Cytokine Delivery. *ACS Nano* **2020**, *14* (9), 11238-11253.
54. Adelmann, C. H.; Traunbauer, A. K.; Chen, B.; Condon, K. J.; Chan, S. H.; Kunchok, T.; Lewis, C. A.; Sabatini, D. M., MFSD12 mediates the import of cysteine into melanosomes and lysosomes. *Nature* **2020,** *588* (7839), 699-704.
55. Stephens, M., False discovery rates: a new deal. *Biostatistics* **2017,** *18* (2), 275-294.
56. R Core Team. R: A language and environment for statistical computing. R Foundation for Statistical Computing. https://www.R-project.org/.
57. Wickham, H., ggplot2: Elegant Graphics for Data Analysis. *Use R* **2009**, 1-212.
58. Tang, Y.; Horikoshi, M.; Li, W. X., ggfortify: Unified Interface to Visualize Statistical Results of Popular R Packages. *R J* **2016,** *8* (2), 474-485.
59. Horikoshi, M.; Tang, Y. ggfortify: Data Visualization Tools for Statistical Analysis Results. https://CRAN.R-project.org/package=ggfortify.

Acknowledgments:

This work was supported in part by SPARC funding at The Broad Institute.

This work was also supported by a grant from the Koch Institute's Marble Center for Cancer Nanomedicine.

This work was supported in part by the Koch Institute Support (core) Grant P30-CA14051 from the National Cancer Institute.

We thank the Koch Institute's Robert A. Swanson (1969) Biotechnology Center for technical support, specifically Flow Cytometry, High Throughput Sciences, and Microscopy cores and the Peterson (1957) Nanotechnology Materials Core Facility.

This work was supported by grants to D.M.S. from the NIH:

R01 CA103866

R01 CA129105

R01 AI047389

U19 AI31151

And a grant from the LEO Foundation.

NB was supported by a Department of Defense Congressionally Directed Medical Research Programs Peer Reviewed Cancer Research Program Horizon Award (W81XWH-19-1-0257).

JPS was supported as a National Institutes of Health grant T32 trainee (CA136432-08) and by the Helen Gurley Brown Presidential Initiative of Dana-Farber Cancer Institute.

D.M.S. is an investigator of the Howard Hughes Medical Institute and an American Cancer Society research professor.

Fellowship support for C.H.A was from the NIH (NRSA F31 CA228241-01).

RRC is a fellow of the Parker B. Francis Foundation.

We would like to thank Todd Golub and Alex Burgin for formative feedback and helpful discussion.

Figure 1A was created in part using Biorender.com

Author contributions:

Conceptualization: NB, JPS

Methodology: NB, JPS, MK

Formal Analysis: NB, JPS, MK, MGR, MR

Investigation: NB, JPS, HCS, MGR

Visualization: NB, JPS

Funding acquisition: NB, JPS, ANK, PTH

Project administration: NB, JPS, MR

Validation: NB, JPS, HCS, CHA, RRC, JHC, HL

Supervision: DMS, JAR, ANK, PTH

Writing – original draft: NB, JPS

Writing – review & editing: NB, JPS, HCS, MK, MGR, MR, CHA, RRC, JHC, HL, DMS, JAR, ANK, PTH

Competing interests: Authors declare that they have no competing interests.

Data and materials availability: All data are available in the main text or the supplementary materials.